Cell Reports
Methods

Article

Understanding how genetically encoded tags and crowding agents affect phase separation by heterochromatin protein HP1α

Graphical abstract

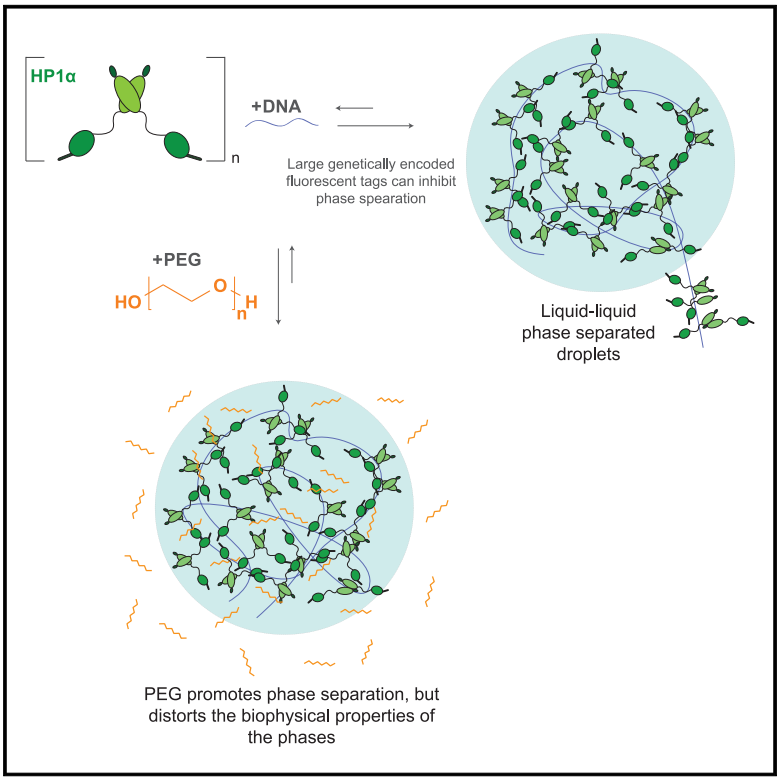

Authors

Ziling (Kate) Zhou, Kibeom Hong, Bo Huang, Geeta J. Narlikar

Correspondence

geeta.narlikar@ucsf.edu

In brief

The phase separation of proteins such as HP1α is typically studied using genetically encoded fluorescent tags in cells and, in many cases, is measured using crowding agents such as PEG *in vitro*. Zhou et al. systematically test how tag size and linker length, as well as the presence of PEG, affect the intrinsic phase separation properties of HP1α *in vitro*.

Highlights

- We show that GFP tags can inhibit phase separation by HP1α
- Tagging with the smaller UnaG tag allows phase separation by HP1α
- Crowding agent PEG dampens the effects of HP1α mutations
- PEG changes the biophysical properties of phase-separated HP1α states

Zhou et al., 2025, Cell Reports Methods 5, 101029
May 19, 2025
https://doi.org/10.1016/j.crmeth.2025.101029

CellPress

Cell Reports Methods

CellPress
OPEN ACCESS

Article

Understanding how genetically encoded tags and crowding agents affect phase separation by heterochromatin protein HP1α

Ziling (Kate) Zhou,[1] Kibeom Hong,[2] Bo Huang,[1,2,3] and Geeta J. Narlikar[1,4,*]
[1]Department of Biochemistry and Biophysics, University of California, San Francisco, San Francisco, CA 94158, USA
[2]Department of Pharmaceutical Chemistry, University of California, San Francisco, San Francisco, CA 94143, USA
[3]Chan Zuckerberg Biohub, San Francisco, San Francisco CA 94158, USA
[4]Lead contact
*Correspondence: geeta.narlikar@ucsf.edu
https://doi.org/10.1016/j.crmeth.2025.101029

MOTIVATION The effects of genetically encoded tags on the intrinsic phase separation behavior of heterochromatin protein 1 alpha (HP1α) have not been systematically studied to date. Moreover, while polyethylene glycol (PEG) has been used in several works to mimic molecular crowding and drive phase separation, the effects of PEG on the properties of the phase-separated states are understudied. To address these gaps, we systematically tested the effects of multiple tags on the ability of HP1α to phase separate *in vitro* and assessed whether and how the presence of PEG affects the intrinsic HP1α interactions that promote phase separation.

SUMMARY

The heterochromatin protein HP1α (heterochromatin protein 1 alpha) phase separates *in vitro* and displays properties compatible with phase separation in cells. Phase separation of HP1α in cells is typically studied using genetically encoded fluorescent tags such as green fluorescent protein (GFP). Whether such tags affect the intrinsic phase separation properties of HP1α is understudied. We assessed how tag size and linker length affect phase separation by HP1α *in vitro*. GFP tags inhibited phase separation by HP1α. In contrast, an UnaG tag with a 16 amino acid glycine-glycine-serine (GGS) linker minimally perturbed HP1α phase separation *in vitro* and could be used to visualize HP1α dynamics in cells. We further investigated the effects of a commonly used crowding agent, polyethylene glycol (PEG). PEG induced phase separation of proteins with no propensity to phase separate under physiological buffer conditions and dampened the effects of HP1α mutations. Therefore, phase separation of biological macromolecules with PEG-containing crowding agents should be interpreted with caution.

INTRODUCTION

The cell is a crowded space consisting of different intracellular organelles that are involved in distinct physiological processes.[1] The cell utilizes membrane-bound organelles such as the nucleus to temporally and spatially separate biochemical reactions. There are also other cellular compartments that are not membrane bound, such as P-bodies and nucleoli in the cytoplasm and nucleus, respectively.[2,3] Such membrane-less organelles are thought to form through the process of liquid-liquid phase separation (LLPS), which results in puncta formation in cells and droplets *in vitro*.[4] LLPS is driven by weak multivalent interactions between macromolecules. Many factors play important roles in the promotion of LLPS, including the modularity of protein domains, polymer multivalency, and the presence of intrinsically disordered regions (IDRs).[5]

Chromatin compartmentalization via LLPS in the nucleus has been implicated in regulating gene expression.[6] Many proteins involved in this process have an intrinsic ability to form droplets *in vitro*. HP1α is involved in gene silencing by compacting and spatially segregating heterochromatin.[7–10] *In vitro*, HP1α can undergo LLPS when its N terminus is phosphorylated or when it interacts with DNA.[8] However, the role of phase separation by HP1α in heterochromatin structure and function *in vivo* is not well understood. Visualizing HP1α dynamics in cells is important for understanding how HP1α-mediated droplets *in vitro* relate to *in vivo* function. To enable such visualization, prior studies have genetically encoded fluorescent tags on HP1α in cells.[7,10–13] However, the introduction of a large tag could affect the multivalent interactions between HP1α molecules that drive phase separation. Indeed, it has been shown that the addition of a GFP tag to either the N or C terminus of phosphorylated HP1α inhibits its

ability to phase separate *in vitro*.[8] This raises the question of whether tagged HP1α retains its native functions and interactions in a cell. It is, therefore, crucial to identify a tagging arrangement on HP1α that minimally perturbs its biophysical properties *in vitro*, as this will allow for a more rigorous interpretation of *in vivo* results.

It is currently unclear whether the inhibitory effects of a GFP tag on HP1α reflect a general consequence of adding a tag or whether there are alternative arrangements of tags that can permit phase separation at concentrations similar to untagged HP1α.[8] To investigate this possibility, we systematically examined the effects of different C-terminal fluorescent tags (auxin-inducible degron-superfolder GFP [AID-sfGFP], monomeric EGFP [mEGFP], and UnaG) on HP1α's phase separation ability *in vitro* (Figure 1).[14,15] These tags vary in size (13–52 kDa). We further varied the length of the unstructured hydrophilic GGS linker (8–16 amino acids [aa]) used to separate the tag from HP1α.

Within our series of tags, the smallest fluorescent tag, UnaG (13 kDa), with a 16 aa linker, was the only tag that minimally perturbed HP1α's phase separation *in vitro*. However, larger tags that inhibit *in vitro* phase separation can still form puncta in a cell.[11,12] We reasoned that this discrepancy could be explained by cellular crowding. To recapitulate cellular crowding, we introduced a commonly used crowding agent, polyethylene glycol (PEG).[16–18] We found that PEG induces phase separation of HP1α constructs that do not intrinsically phase separate in physiological buffer conditions. Overall, our findings highlight the need to quantitatively test the phase separation effects of fluorescent tags used to visualize HP1α in cells and raise questions about the biological relevance of phase-separated condensates induced with PEG.

RESULTS

Effects of tag size and linker length on phase separation of HP1α

HP1α has a domain architecture, as shown in Figure 1A. The protein has two structured domains: the chromoshadow domain (CSD) and the chromodomain (CD). The CSD is responsible for homodimerization, and the CD recognizes the H3K9me2/3 mark on chromatin. The CSD and CD are connected by an IDR, termed the hinge, that binds to nucleic acids. Two additional IDRs are present on the N and C termini of the protein and are termed the N-terminal extension (NTE) and the C-terminal extension (CTE), respectively. Previous work has suggested that HP1α phase separates through interactions between the NTE and the hinge.[8,19] Additionally, the CTE interacts with the hinge domain in the absence of DNA to autoinhibit oligomerization.[8] Truncation of the NTE substantially inhibits HP1α's phase separation, while deletion of the CTE promotes HP1α's phase separation.[19] The need for an intact NTE to allow phase separation suggested that a tag would be better tolerated on the CTE. Therefore, all tags for this study were placed on the C terminus of HP1α.

Of the many variables related to a tag that could affect the ability of HP1α to phase separate, we focused on two: the size of the tag and the length of the linker. We reasoned that varying these two features would vary the extent of steric hindrance for the dynamic higher-order interactions required to drive phase separation. To address the effect of tag size, we chose two tags, mEGFP (27 kDa) and UnaG (13 kDa). We chose mEGFP to avoid the complication of GFP dimerization, as that could have confounding effects on phase separation. To address the linker length effect, we tested linker lengths of 8 and 16 aa. We uncoupled the effects of tag size and linker length by designing four tagged HP1α constructs (HP1α-8aa-mEGFP, HP1α-16aa-mEGFP, HP1α-8aa-UnaG, and HP1α-16aa-UnaG) (Figure 1A).

We performed phase separation assays in the presence of a 2.7 kbp plasmid DNA using a defined series of HP1α concentrations.[19] Within this series, we defined the saturation concentration for phase separation as the lowest concentration of HP1α at which we can detect droplet formation via microscopy. In a complementary assay, we used turbidity as measured by absorbance at 340 nm (Figure S4). Overall, the saturation concentrations obtained for the mEGFP- and UnaG-tagged constructs by the turbidity assay were within 3-fold of those obtained by visual inspection of droplet formation (Tables S3 and S4). We compared phase separation in the following buffer conditions: 20 mM HEPES, 70 mM KCl, and 1 mM DTT. As previously reported, unlabeled HP1α readily undergoes phase separation with the 2.7 kbp DNA construct, phase separating at a saturation concentration of 3.3 μM (Figure 1B, Tables 1 and S3).[19] In addition to untagged HP1α, we also chemically labeled HP1α. We attached a KCK tag to the C terminus of HP1α and labeled the cysteine residue with Atto488 using maleimide chemistry. HP1α-KCK-Atto488 also displayed a saturation concentration of 3.3 μM, indicating that the chemically attached label does not perturb the phase separation properties of HP1α (Figure 1C). In contrast, HP1α-16aa-mEGFP remains soluble at high micromolar concentrations (450 μM) (Figure 1D). With a shorter linker of 8 aa, HP1α-8aa-mEGFP forms non-spherical-shaped phases at a saturation concentration of 250 μM (Figure 1E). This is 75-fold higher than the saturation concentration of wild-type (WT) HP1α. These results indicate that a C-terminal mEGFP tag substantially interferes with the phase separation behavior of HP1α, independent of linker length. To test if the mEGFP tag affects the binding of HP1α to DNA, we measured the binding of mEGFP-tagged HP1α to a 187 bp stretch of DNA by electrophoretic mobility shift assays (EMSAs) (Figures S1C and S1D). The concentration at which half the DNA is bound is called the $K_{1/2}$ value. These values for untagged HP1α and HP1α-16aa-mEGFP are 0.88 and 0.58 μM, respectively (Figures S1C–S1F). The similar $K_{1/2}$ values suggest that the mEGFP tag does not interfere with DNA binding but may affect the oligomerization of HP1α. Interestingly, HP1α-16aa-mEGFP can be incorporated into droplets pre-formed by untagged HP1α and DNA up to stoichiometric levels (Figures S5A and S5B). However, beyond a 1:1 M ratio, additional HP1α-16aa-mEGFP dissolves the droplet.

Next, we evaluated the effects of the smaller UnaG tag. The UnaG protein shows fluorescent properties upon binding a cofactor, bilirubin (Br).[15] Therefore, we tested the effects of the UnaG tag with (holo) and without (apo) its cofactor, Br, and connected via either an 8 or 16 aa linker. Without Br, HP1α-16aa-(apo)UnaG and HP1α-8aa-(apo)UnaG phase separate with saturation concentrations of 6.5 and 4.7 μM, respectively (Figures S1A and S1B). These values are comparable to the

CellPress
OPEN ACCESS

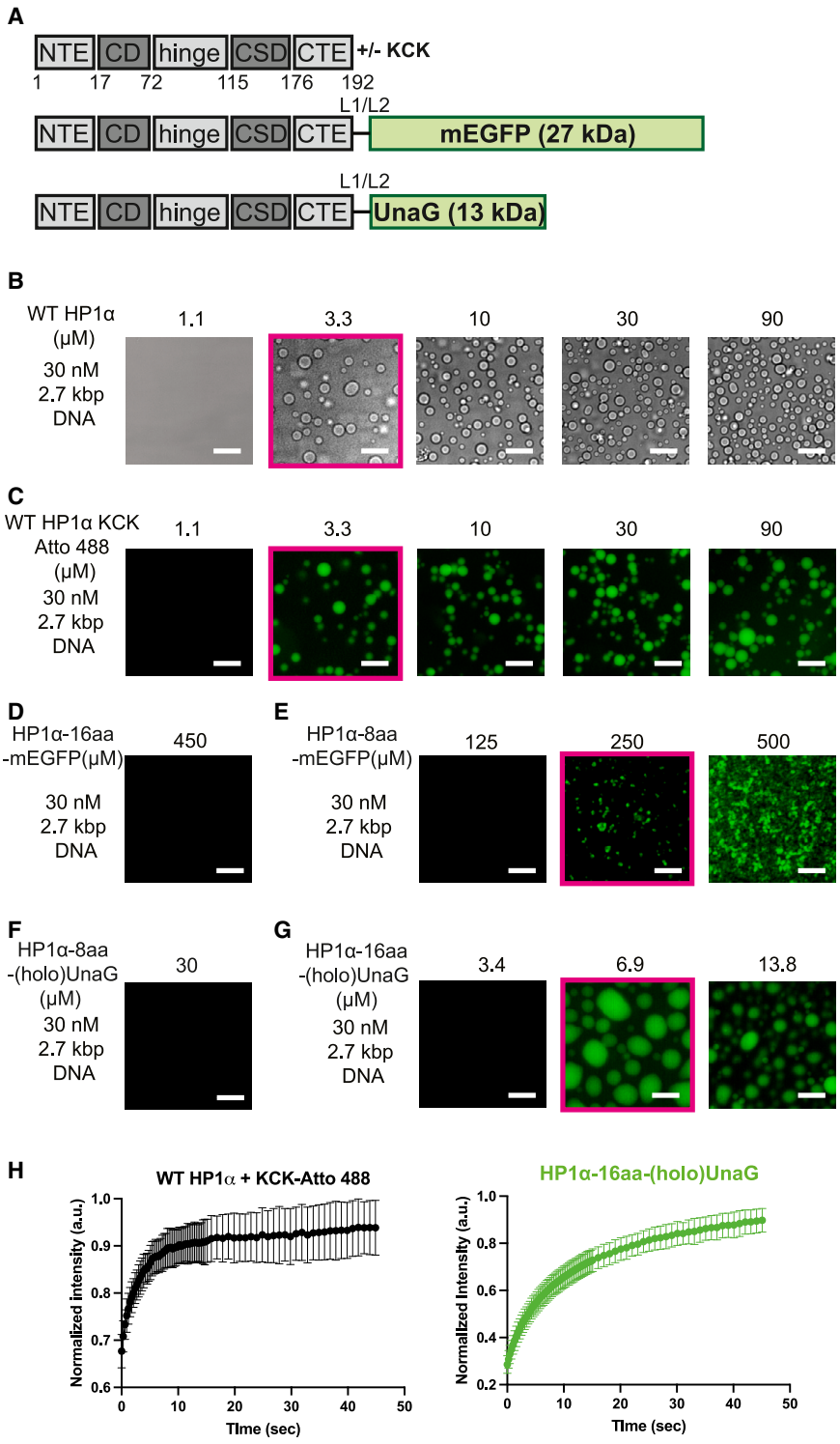

Figure 1. Tag size and linker length influence HP1α's phase separation properties *in vitro*

(A) Domain diagrams of WT HP1α with or without tags. L1 and L2 represent linker lengths of 8 and 16 amino acids, respectively. The sequences of the linkers are GSGGSGGS and GSGGSGGS GSGGSGGS.

(B) Bright-field images of a concentration series of WT HP1α with 30 nM of 2.7 kbp DNA. The red box indicates the saturation concentration for phase separation.

(C) Fluorescent images of a concentration series of HP1α-KCK-Atto488 (1 KCK:50 WT) with 2.7 kbp DNA.

(D) Fluorescent image of 450 μM HP1α-16aa-mEGFP with 2.7 kbp DNA.

(E) HP1α-8aa-mEGFP with 2.7 kbp DNA.

(F) Fluorescent image of HP1α-8aa-(holo)UnaG mixed with 2.7 kbp DNA.

(G) Fluorescent images of concentration series of HP1α-16aa-(holo)UnaG with 2.7 kbp DNA.

(H) FRAP analysis of WT HP1α (left) and HP1α-16aa-(holo)UnaG (right) condensates.

For each data point, the standard deviation for $n = 8$ is shown. Scale bars represent 20 μm.

saturation concentrations of WT HP1α, suggesting that the apo form of UnaG minimally perturbs HP1α's phase separation function. However, in the holo form, HP1α-8aa-(holo)UnaG does not phase separate up to concentrations as high as 30 μM (Figure 1F). In contrast, HP1α-16aa-(holo)UnaG shows a similar saturation concentration (6.5 μM) as the apo form (Figure 1G and Table S3). Thus, in the series tested above, the least perturbative fluorescent tagging arrangement for HP1α is HP1α-16aa-(holo)UnaG.

We next assessed whether the UnaG tag affected the dynamics of HP1α within the phase-separated droplets. We used fluorescence recovery after photobleaching (FRAP) on phase-separated HP1α-16aa-(holo)UnaG and HP1α-KCK-Atto488 droplets in the presence of DNA. The half-times for recovery of fluorescence in the fast phase are 1.9 and 3.1 s for HP1α-KCK-Atto488 and HP1α-16aa-UnaG, respectively (Figures 1H and S2A). The two constructs also show comparable half-times for recovery of the slow phases (Table 2). These results indicate that this UnaG tag arrangement maintains the seconds-timescale dynamics of HP1α in its phase-separated droplets. The comparison with the mEGFP tag suggests that both tag size and linker length affect HP1α's biophysical properties. Importantly, our studies have identified a specific arrangement of the UnaG tag that minimally perturbs phase separation by HP1α. This tag now allows direct comparison of the behavior of HP1α inside and outside of a cell.

More recently, GFP tags have been combined with degrons to study the effects of rapid protein degradation.[14,20] In the context

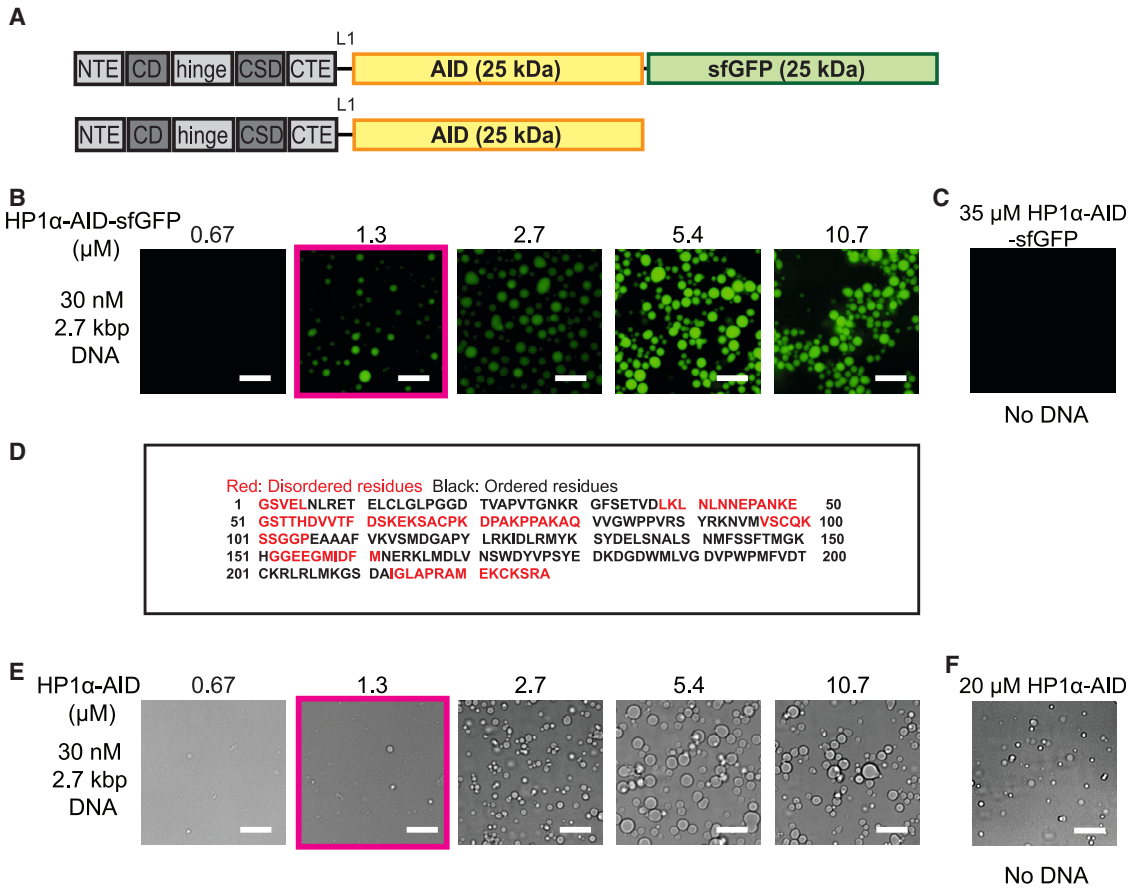

Figure 2. The AID tag promotes phase-separation by HP1α

(A) Domain diagrams of HP1α with 2 different large tags, where L1 represents 8 amino acids, respectively.

(B) Fluorescent microscopy images of a concentration series of HP1α-AID-sfGFP with 30 nM of 2.7 kbp DNA. Red box indicates the saturation concentration for phase separation.

(C) Fluorescent image of 35 μM HP1α-AID-sfGFP without DNA.

(D) Sequence of the AID and disorder prediction from the Protein DisOrder prediction system (PrDOS), where red-colored letters are predicted to be highly disordered and black are predicted to be ordered.

(E) 20× bright-field images of a concentration series of HP1α-AID with 30 nM of 2.7 kbp DNA.

(F) Bright-field microscopy of 20 μM HP1α-AID without DNA.

Scale bars represent 20 μm.

of HP1α, the AID-sfGFP tag has been used to study the effects of rapidly degrading HP1α in cells (Figure 2A). In HP1α-AID-sfGFP, AID and sfGFP combined are 50 kDa, around twice the size of HP1α. We, therefore, hypothesized that similar to mEGFP, this large tag would interfere with HP1α's phase separation ability. Surprisingly, HP1α-AID-sfGFP forms phase-separated droplets in the presence of DNA at a lower saturation concentration (1.3 μM) than untagged HP1α (Figures 2B and 2C, and Table S3). We hypothesized that the AID-sfGFP tag promotes phase separation due to a large IDR contributed by the AID (Figure 2D). To separately test the AID's effect on HP1α phase separation, we generated an HP1α-AID construct (Figure 2A). Unlike untagged HP1α, HP1α-AID now phase separates in the absence of DNA (Figure 2F). Further, HP1α-AID shows the same saturation concentration as HP1α-AID-sfGFP in the presence of DNA (Figure 2E). These results indicate that the AID tag enhances HP1α's intrinsic phase separation ability and potentially rescues some of the inhibition introduced by the GFP tag in cells.

Assessing the effects of tagging HP1α with UnaG in cells

We next assessed whether the HP1α-16aa-UnaG tagging arrangement could be used to study HP1α dynamics in cells. The UnaG tag is more prone to photobleaching during live-cell fluorescence imaging compared to GFP. Hence, we used an engineered and enhanced version of UnaG with a V2L mutation (eUnaG) that is more suitable for live-cell imaging (Figures 3 and S2C).[21] To best control and test the effects of tagging on HP1α, we tagged endogenous HP1α rather than using an overexpression or transient expression approach. We tagged endogenous HP1α on the C terminus with a 16 aa linker and either the UnaG or eUnaG tag in U2OS cells through CRISPR-Cas9 knockin. Notably, the majority of mammalian cells, including U2OS cells,

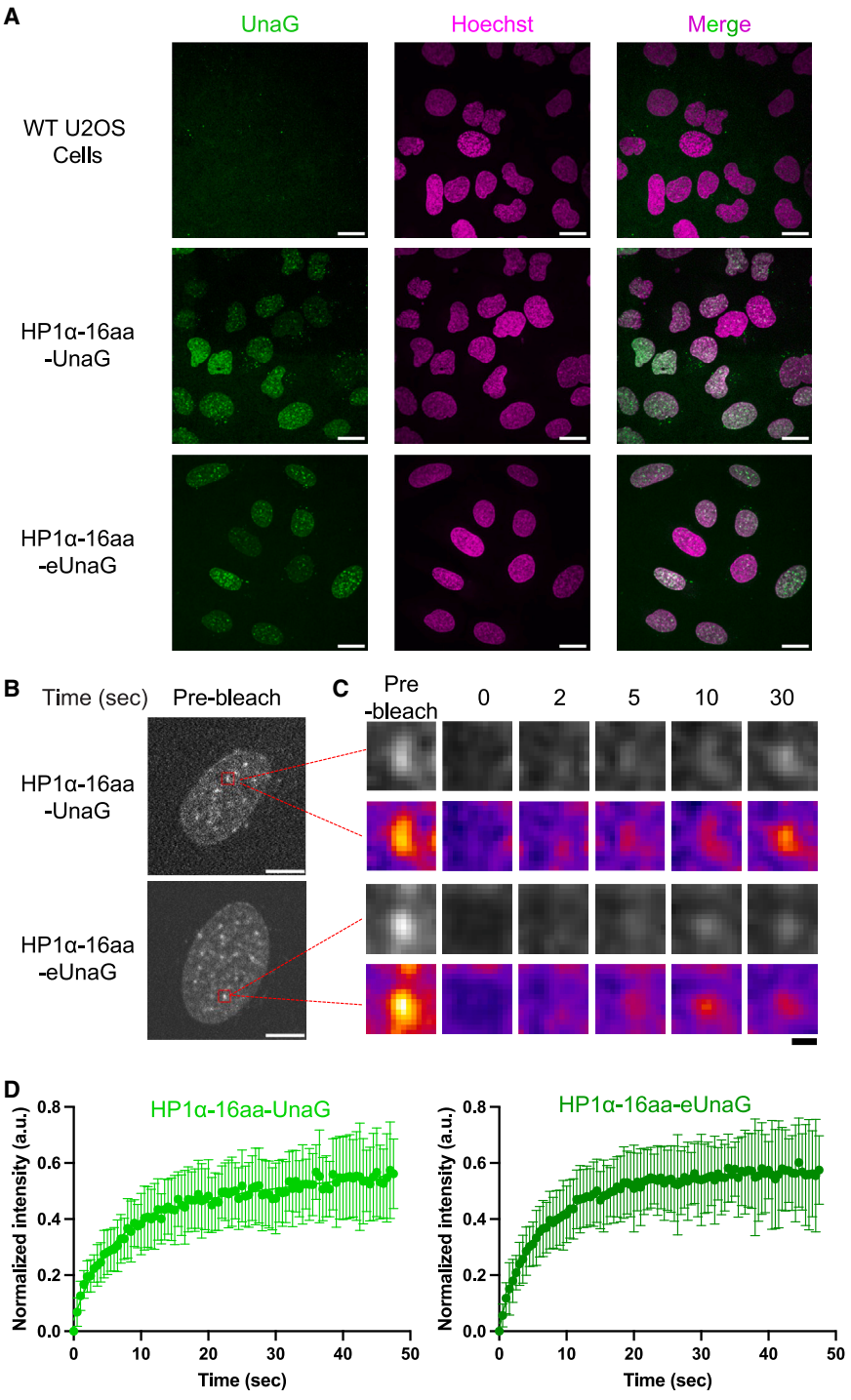

Figure 3. HP1α-16aa-UnaG exhibits second-scale dynamics in cells

(A) Live-cell confocal microscopy images of U2OS WT (top row), HP1α-16aa-UnaG knockin (KI) cells (middle row), and HP1α-16aa-eUnaG KI cells (bottom row) with green fluorescent UnaG or eUnaG signals (left column) and Hoechst DNA stain from nucleus (middle column) and overlay images of both channels of green fluorescent UnaG or eUnaG (right column, green) and Hoechst DNA stain (right column, magenta) Scale bars represent 20 μm.

(B) Examples of cells with HP1α-16aa-UnaG KI (top) and HP1α-16aa-eUnaG KI (bottom) for live-cell FRAP experiments prior to heterochromatin puncta photobleaching. Scale bars represent 10 μm.

(C) Magnified images of inset photobleached HP1α-16aa-UnaG (top) and HP1α-16aa-eUnaG (bottom) heterochromatin puncta at different time points upon heterochromatin puncta photobleaching. Grayscale and a fire lookup table (LUT) are applied to visualize the intensity level of UnaG and eUnaG intensities. Scale bar represents 1 μm.

(D) FRAP quantification of both HP1α-16aa-UnaG (left) and HP1α-16aa-eUnaG (right) puncta.

For each data point, the standard deviation for $n = 22$ is shown.

produce the UnaG ligand bilirubin endogenously, allowing the UnaG tags to be in the holo-bound state without exogenous bilirubin addition. In live-cell imaging, both UnaG- and eUnaG-tagged HP1α proteins were found to be enriched in puncta that co-localized with concentrated DNA staining, consistent with the puncta representing heterochromatin (Figure 3A). We then determined the dynamics of endogenous HP1α tagged with UnaG or eUnaG. FRAP experiments carried out on HP1α puncta in U2OS cells showed comparable recovery for both tags (<2-fold change), indicating there is no significant difference between UnaG and eUnaG tags on HP1α dynamics *in vivo* (Figures 3B–3D). Importantly, the bleached puncta reached 56.9%–67.5% of their starting intensity within seconds, similar to previously reported findings (Table S2).[11–13] These results, together with the results in the previous section, indicate that the HP1α-16aa-UnaG/eUnaG tagging arrangement can be used to study the dynamics and potential phase separation properties of HP1α in cells without disrupting its intrinsic biophysical properties.

Testing the effect of PEG8000 on phase separation properties

Interestingly, even though previous studies and our studies here show that a GFP tag inhibits phase separation by HP1α, GFP-tagged HP1α constructs have been shown to be components of dynamic heterochromatin puncta *in vivo*.[11,13,22–24] It is possible that phase separation of these tagged HP1α proteins in cells is promoted by other cellular contents and by the high degree of molecular crowding. To mimic cellular crowding *in vitro*, we used PEG, a commonly used

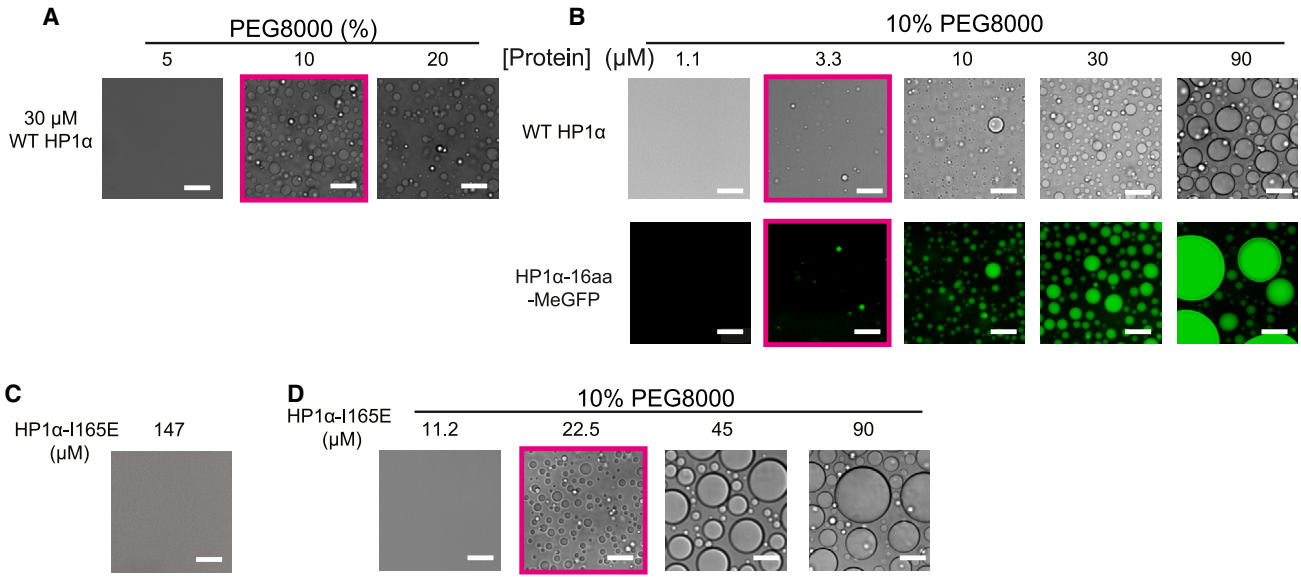

Figure 4. PEG8000 induces phase separation of HP1α and tagged constructs in the absence of DNA

(A) Three different PEG8000 percentages were used to determine the minimum PEG percentage (10%) needed to induce HP1α phase separation without DNA.

(B) Concentration series of HP1α and HP1α-16aa-mEGFP with 10% PEG8000. Red box represents the saturation concentration for phase separation.

(C) Bright-field image of HP1α CSDm alone at 147 μM with no visible droplets.

(D) Bright-field images of a concentration series of HP1α CSDm with 10% PEG8000. HP1α CSDm displays phase separation with a saturation concentration of 22.5 μM.

Scale bars represent 20 μm.

water-soluble macromolecular crowding agent. We tested two different PEG molecules (PEG8000 and PEG4000).

We first determined if PEG8000 promotes phase separation of HP1α without DNA. We titrated PEG and found that 10% is sufficient for HP1α to phase separate on its own (Figure 4A). This percentage of PEG is similar to that used in previous studies.[16,17,25–27] In the absence of PEG, HP1α alone does not phase separate at concentrations up to 800 μM.[8,19] However, adding 10% PEG8000 lowered HP1α's saturation concentration to 3.3 μM (Figure 4B and Table S4). Analogously, PEG also enables HP1α-16aa-mEGFP to phase separate at 3.3 μM without DNA (Figure 4B). To find a negative control, we used an HP1α protein with a chromoshadow domain mutation (CSDm). This mutation inhibits HP1α dimerization, and the HP1α CSDm protein does not phase separate with the 2.7 kb DNA construct, even at 147 μM (Figure 4C).[8] However, PEG induces phase separation of HP1α CSDm in the absence of DNA and at a saturation concentration of 22.5 μM, which is only 6.8-fold higher than the other HP1α constructs above (Figure 4D).

Since PEG is also known to precipitate DNA, we investigated how it affects the phase separation of HP1α in the presence of DNA. Bright-field microscopy revealed that under the conditions of our experiments, PEG8000 does not promote phase separation of DNA alone (Figure 5B). In the presence of PEG, DNA does not further lower the saturation concentration of untagged HP1α (Figure 5A). For HP1α-16aa-mEGFP, the addition of DNA also did not decrease the saturation concentration in comparison to PEG and protein alone (Figure 5A). These results suggest that PEG8000 alters the protein-protein and protein-nucleic acid interactions within the droplets. We next studied the effect of PEG8000 on the HP1α CSDm with DNA since PEG induced phase separation of HP1α CSDm alone. We found that in the presence of PEG8000, HP1α CSDm now phase separates at 5.6 μM, an 4-fold lower concentration than in the absence of DNA (Figure 5F).

To further investigate the effects of PEG on phase separation, we used both partial- and whole-droplet FRAP on the droplets pre-formed with HP1α-KCK-Atto488 and DNA in the presence of 10% PEG8000. In the presence of PEG8000, only 56% of the bleached fluorescence recovered over the timescale of the experiment upon bleaching a portion of the droplet, in contrast to 99% recovery observed in the absence of PEG8000 (Figures 5C and S2B vs. Figure 1H; Table 2). FRAP experiments on droplets formed with HP1α-KCK-Atto488 alone in the presence of PEG8000 showed an even smaller fraction of fluorescence recovery (Figures 5C and S2B; Table 2). Whole-droplet FRAP experiments further indicated that PEG interferes with HP1α diffusion within droplets and between its surrounding environments. We found that droplets formed in the presence of 10% PEG8000, when bleached completely, only recovered up to 12.45% of the original fluorescence at 150 s post-bleaching (Figures 5D and 5E; Table S1). In contrast, when we completely bleached droplets formed from HP1α-KCK-Atto488 and DNA, these recovered 93% of the original fluorescence on the seconds timescale (Table S1 and Figures 5D and 5E). These results suggest that 10% PEG8000 substantially changes the dynamics of the HP1α proteins within the phase-separated droplets (Figures 5C–5E; Tables 2 and S1).

CellPress
OPEN ACCESS

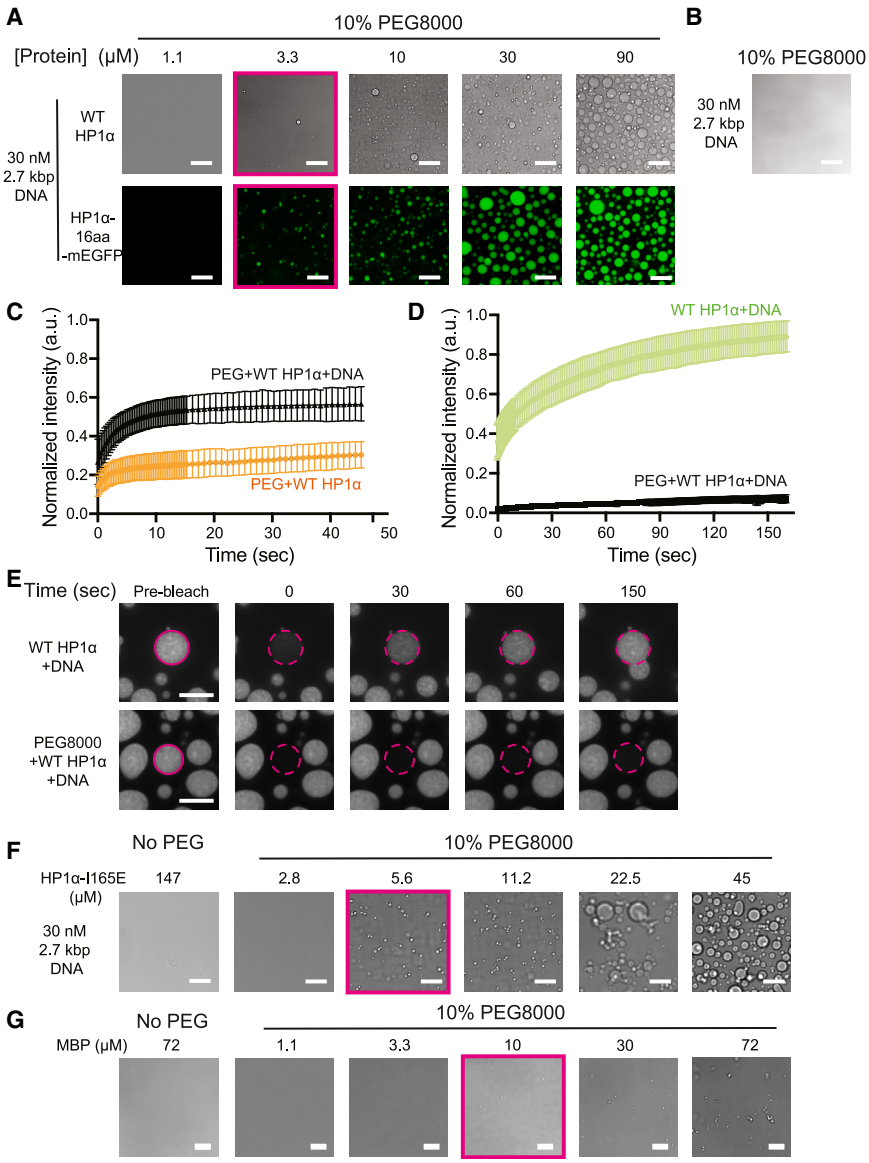

Figure 5. PEG8000 diminishes the effects of DNA in promoting phase separation

(A) Concentration series of HP1α with 30 nM of 2.7 kbp DNA and 10% PEG8000. Scale bars represent 20 μm. Red box indicates the saturation concentration for phase separation.

(B) 10% PEG8000 with 30 nM of 2.7 kbp DNA.

(C) Quantification of FRAP of PEG8000-induced HP1α-KCK-Atto488 and HP1α-KCK-Atto488 plus DNA droplets. For each data point, the standard deviation for $n = 8$ is shown.

(D) Quantification of whole-droplet FRAP of HP1α-KCK-Atto488 with 30 nM of 2.7 kbp DNA droplets and PEG8000-induced HP1α-KCK-Atto488 plus DNA droplets. For each data point, the standard deviation for $n = 12$ is shown.

(E) Confocal images of HP1α-KCK-Atto488 with 30 nM of 2.7 kbp DNA droplets and PEG8000-induced HP1α-KCK-Atto488 plus DNA droplets at different time points pre- and post-FRAP. Solid and dashed line circles represent pre- and post-bleaching, respectively. Scale bars represent 10 μm.

(F) Left, bright-field image of 147 μM HP1α CSDm with 30 nM of 2.7 kbp DNA with no PEG8000. Right, a concentration series of HP1α CSDm with 30 nM of 2.7 kbp DNA with 10% PEG8000. Scale bars represent 20 μm.

(G) Left, maltose-binding protein alone at 72 μM. Right, concentration series of MBP with 10% PEG8000. Condensates are visible around 10 μM. Scale bars represent 10 μm.

Given that all the constructs we tested contain IDRs, which often promote phase separation, we wanted to test the effects of PEG on a protein that lacks IDRs. We, therefore, chose maltose-binding protein (MBP), which is a canonical globular protein often used to solubilize other proteins. Interestingly, we observed phase separation of MBP in the presence of PEG, starting at 10 μM MBP (3-fold higher than HP1α and HP1α-16aa-mEGFP but 2-fold lower than HP1α CSDm) (Figure 5G; Table 1).

PEG4000 leads to phase separation of protein, similar to the effects of PEG8000

We also used PEG4000 in addition to PEG8000 to see if PEG at a lower molecular weight has distinct effects on phase separation. We used 10% PEG4000 throughout the assays to keep our comparisons under the same conditions. With 10% PEG4000, untagged HP1α phase separates at 3.3 μM with and without DNA, while HP1α-16aa-mEGFP alone has a saturation concentration of 1.1 μM (Table 1; Figure S3A). Similar to 10% PEG8000, 10% PEG4000 is not sufficient to induce phase separation of DNA alone (Figure S3C). In the presence of 10% PEG4000, HP1α CSDm phase separates with and without DNA at 10 and 30 μM, respectively (Figures S3D and S3E). Our findings imply that both PEG4000 and PEG8000 can induce the phase separation of many types of proteins irrespective of their ability to phase separate without PEG. Furthermore, under conditions containing PEG, HP1α proteins show a substantially reduced dependence on DNA for promoting phase separation.

DISCUSSION

Understanding how the phase separation behavior of proteins contributes to biological function requires an ability to visualize the dynamics of the corresponding proteins in cells. A common and powerful way of studying such dynamics relies on tagging the protein of interest with a genetically encoded fluorescent tag. However, the addition of the tag has the potential to perturb the intrinsic phase separation properties of the protein. Here, we sought to identify a genetically encoded tagging arrangement for the heterochromatin protein HP1α that would minimally perturb

Table 1. Saturation concentration (μM) of different proteins alone or proteins plus 2.7 kbp DNA with and without crowding agents PEG8000 and PEG4000 measured by light microscopy, respectively

Crowding agent	Protein alone				Protein + DNA		
	WT HP1α (μM)	WT HP1α-*I165E* (μM)	HP1α-16aa-mEGFP (μM)	MBP (μM)	WT HP1α (μM)	WT HP1α-*I165E* (μM)	HP1α-16aa-mEGFP (μM)
None	>400	>150	>500	>80	3.3	>150	>450
10% PEG8000	3.3	22.5	3.3	10	3.3	5.6	3.3
10% PEG4000	3.3	30	1.1	–	3.3	10	–

its phase separation properties *in vitro*. We found that both the linker length and the size of the tag matter in designing such a tagging arrangement. Through this study, we have identified one minimally perturbative tagging arrangement for HP1α, a C-terminal (holo)UnaG tag (13 kDa) with a 16 aa GS-rich linker. We have further investigated the effects of PEG-based crowding agents to assess whether mimicking the molecular crowding in the nucleus can increase the repertoire of genetically encoded tags that allow HP1α phase separation with comparable properties as untagged HP1α. Below, we discuss the implications of our study for understanding biological phase separation.

In the context of C-terminally tagging HP1α, we find that the commonly used GFP class of tags interferes with phase separation irrespective of whether we use an 8 or 16 aa linker. We recognize that a more exhaustive search of linker lengths would be required to rule out mEGFP as an appropriate tag. However, our results show that HP1α-16aa-(holo)UnaG allows phase separation with comparable properties as untagged or chemically tagged HP1α, suggesting that the larger size of mEGFP compared to (holo)UnaG is responsible for the perturbative effects of the mEGFP-tagging arrangements. The HP1α-16aa-(holo)UnaG construct phase separates with a 2.7 kbp plasmid DNA at a saturation concentration of 6.9 μM, which is within 3-fold of the saturation concentration observed with untagged HP1α (Figures 1B and 1G). Our FRAP studies indicate that HP1α-16aa-(holo)UnaG also has comparable dynamics to chemically tagged HP1α within the phases. While HP1α-16aa-(holo)UnaG shows a smaller fraction of fluorescence that recovers in the fast phase compared to chemically tagged HP1α, overall, the bleached spot recovers up to 94% of the initial fluorescence within seconds (Table 2). While size is one difference between UnaG and mEGFP, it is possible that differences in other features between the two tags, such as surface charge distribution and solubility, also contribute to their differential effects on the phase separation of HP1α.

Interestingly, the mEGFP tag did not interfere with DNA binding (Figures S1C and S1D), suggesting that the tag inhibits the higher-order HP1α oligomerization that is essential for phase separation. Additionally, we uncovered some differences in the effects of the apo vs. holo versions of the UnaG tag. Specifically, whereas HP1α-8aa-(apo)UnaG phase separates at a comparable saturation concentration to untagged HP1α, the HP1α-8aa-(holo)UnaG protein does not phase separate up to 30 μM. While we do not understand the basis for this difference, we speculate that the holo form of UnaG causes a larger steric hindrance compared to the apo form and that extending the linker length to 16 aa relieves this steric hindrance. Consistent with this possibility, the secondary structure of holo UnaG shows that it is a well-folded beta-barrel protein, and it is possible that without the Br cofactor, UnaG is less structured.[15] This potential of the disordered nature of tags affecting phase separation is also exemplified by our finding that the AID tag promotes the phase separation of HP1α. This result is consistent with the patches of disorder predicted in the sequence of the AID. The binding of auxin presumably structures the AID tag.

Testing the HP1α-16aa-(holo)-UnaG tagging arrangement in cells using endogenously tagged HP1α shows that tagged protein is concentrated into puncta that are also enriched for DNA, suggesting that the tag is compatible with heterochromatin formation. Further, the tagged HP1α recovers with rapid kinetics comparable to the kinetics of recovery observed *in vitro* (Figures 1H and 3D). These recovery kinetics are also comparable to previously reported recovery kinetics for exogenously expressed GFP-tagged human HP1α in CHO cells.[11] The comparable recovery kinetics are consistent with our observation that mEGFP-tagged HP1α binds DNA with a similar affinity to untagged HP1α and our interpretation that the mEGFP tag affects the oligomerization of HP1α.

To the best of our knowledge, there is only one study in the literature that reports a homozygous knockin of HP1α with a large (>13 kDa) fluorescent tag. This is the study with the homozygous knockin of HP1α-AID-sfGFP in U2OS cells, the one construct with a large tag that we show here phase separates at a relatively similar saturation concentration to untagged HP1α *in vitro* (Figures 1B and 2B).[14] This raises the possibility that homogeneous knockin is only achievable if the tag of interest does not affect HP1α phase separation *in vitro*. Such a possibility underscores the importance of using *in vitro* experiments to validate the functional relevance in cells. Our knockin cell line may provide a useful tool to further study the diffusion of HP1α and its association with heterochromatin. More generally, we hope the results with UnaG prompt experts in genetically encoded fluorescent tags to seek and develop other small fluorescent tags that are stable and less prone to photobleaching. Overall, our results showcase that understanding the biophysical effects of tags on the protein of interest is critical when choosing tags for studying phase separation in cells. Each protein is expected to have a different tolerance for tags, and proteins such as HP1α with N- and C-terminal IDRs that participate in multivalent interactions may be more intolerant of tags in the context of phase separation.

For HP1α with large tags that cannot phase separate *in vitro* but can get recruited to heterochromatic sites in cells, this may be due to three possibilities. First, the untagged HP1α could

Table 2. Partial-droplet FRAP data of 5 conditions tested: HP1α-KCK-Atto488 with 2.7 kbp DNA, HP1α-16aa-(holo)UnaG with 2.7 kbp DNA, HP1α-KCK-Atto488 with 10% PEG8000, and HP1α-KCK-Atto488 with 2.7 kbp DNA and 10% PEG8000, respectively (*n* = 8)

	WT HP1α KCK + DNA	HP1α-16aa-(holo)UnaG	WT HP1α KCK + PEG8000	WT HP1α KCK + DNA+ PEG8000
Fast half-life (s)	1.9	3.1	1.3	2.4
Slow half-life (s)	55.9	21.1	300.9	278.5
Percent fast (%)	65.5	38.0	9.8	33.42
Percent recovery after plateau reached (%)	99	94.07	36.4 (did not plateau)	56.6

These values were derived from the data in Figures 5 and S2.

recruit and organize exogenously expressed tagged HP1α proteins into puncta. Such a possibility is supported by our observation that droplets made with untagged HP1α and DNA can accommodate GFP-tagged HP1α (Figures S5A and S5B). Second, interactions with other heterochromatin components may compensate for defects in the phase separation of tagged HP1α. Third, the molecular crowding in the nucleus may facilitate phase separation and compensate for the inhibition introduced by the tag. Here, we studied the third possibility by testing PEG8000 and PEG4000, reagents that are commonly used to mimic molecular crowding *in vitro*. We found that the presence of PEG promotes the phase separation of HP1α when tagged with proteins larger than UnaG. However, the presence of PEG also greatly diminished the contributions of two types of biologically relevant interactions. First, the phase separation of HP1α was no longer reliant on the presence of DNA. Second, mutating the CSD-CSD interface in HP1α, which inhibits the phase separation of HP1α and raises the saturation concentration by at least 40-fold, now raises the saturation concentration by only 6-fold.

If PEG simply increased the local concentration of HP1α and DNA, then we would have expected the saturation concentrations for both the WT and CSDm HP1α to decrease but the difference to remain at least 40-fold. The observation that the difference between the saturation concentrations of WT and CSDm HP1α is reduced to 6-fold suggests that the types of inter-molecular interactions with and without PEG are different. Consistent with this possibility, our FRAP studies indicate that a smaller population of bleached HP1α molecules recover in the presence of PEG. Prior work has shown that when part of a droplet formed from HP1α-KCK-Atto488 and DNA is subjected to photobleaching, the recovery of fluorescence occurs on the order of seconds without a substantial decrease in the total intensity of the droplet. This result implies that HP1α molecules can exchange on the order of seconds between droplets. However, we find that in the presence of PEG, the total intensity of the droplet decreases during recovery of the photobleached region (Figure S2B). This difference suggests that in the presence of PEG, the exchange of HP1α molecules between droplets is much slower than within a droplet.

Overall, our results suggest that PEG alters the protein-protein and protein-DNA networks within condensates and does not simply act as an inert crowding agent. Our studies thus suggest that *in vitro* phase separation studies carried out in the presence of PEG should be interpreted with caution. Our findings are consistent with previous studies that have shown that PEG partitions within NPM1 and rRNA droplets and decreases the mobile fraction of protein within the condensates and more recent studies showing that PEG8000 can drive the phase separation of a wide range of proteins.[16,18] Therefore, as suggested in these previous studies, it is important to assess the biological relevance of PEG-induced phase separation with caution. Further, PEG may not be able to recapitulate the complexity of the diverse components in a cell. Such added complexity of other interacting components is also likely to change the saturation concentration. Indeed, recent studies show that the saturation concentration of a fluorescently tagged N-Myc protein is 400 nM in mammalian cells but at least 10-fold higher *in vitro*.[28] Thus, despite the ambiguity of using PEG *in vitro*, the need to find estimates of how macromolecular crowding in cells affects saturation concentrations remains. We anticipate that further method development will be required for such estimates.

Limitations of the study

Our study investigates how specific tags on HP1α correlate with condensate formation *in vitro* and in cells. However, we do not measure the effects of the tagged HP1α constructs on any other phenotypic outcomes, such as gene expression. This is a limitation of the study because, in principle, it is possible that while condensate formation is disrupted, gene expression is not.

RESOURCE AVAILABILITY

Lead contact

Requests for further information and resources should be directed to and will be fulfilled by the lead contact, Geeta J. Narlikar (geeta.narlikar@ucsf.edu).

Materials availability

Plasmids generated in this study are available from the lead contact with a completed materials transfer agreement.

Data and code availability

- All raw and quantified data reported in this paper will be shared by the lead contact upon request.
- This paper does not report original code.
- Any additional information required to reanalyze the data reported in this paper is available from the lead contact upon request.

ACKNOWLEDGMENTS

We thank Upneet Kaur for the helpful guidance on writing the manuscript and the experimental design. We thank Emily Wong for the experimental setup, CBX5 plasmid, and HP1α-KCK-Atto488. We thank Julia Tretyakova for the large-scale purification of the 2.7 kbp plasmid. We thank Upneet Kaur and Elise Muñoz for the Cy5-labeled 187 bp DNA. We thank Soyeon Kim from

the Center for Advanced Light Microscopy (CALM) at UCSF for training on microscopes and troubleshooting. We thank Klaus Yserentant for *in vivo* FRAP analysis and guidance for ImageJ macro script writing. We thank Dr. Xiaokun Shu for suggesting the use of the UnaG tag and for feedback on the manuscript. We thank Emily Wong and Camille Moore for helpful feedback on the manuscript and the Narlikar lab for stimulating discussions during this study. This research was funded by grants from the NIH to G.J.N. (U01DK127421 and R35GM127020) and B.H. (U01DK127421) and grants to G.J.N. from the NSF (#1921794) and the Sandler Program for Breakthrough Biomedical Research, which is partially funded by the Sandler Foundation. B.H. is a Chan-Zuckerberg Biohub, San Francisco Investigator.

AUTHOR CONTRIBUTIONS

Z.K.Z. generated the various tagged constructs, purified the corresponding proteins, and performed all biochemical experiments; K.H. tagged cellular HP1α and performed all the cellular experiments; B.H. provided guidance on the cellular experiments; G.J.N. conceived and oversaw the project; and all authors participated in the interpretation and discussion of the results and writing of the manuscript.

DECLARATION OF INTERESTS

G.J.N. is a co-founder and member of the scientific advisory board of TippingPoint Biosciences.

DECLARATION OF GENERATIVE AI AND AI-ASSISTED TECHNOLOGIES IN THE WRITING PROCESS

During the preparation of this work, the authors used Grammarly in order to check spelling and grammatical errors. After using this tool/service, the authors reviewed and edited the content as needed and take full responsibility for the content of the publication.

STAR★METHODS

Detailed methods are provided in the online version of this paper and include the following:

- KEY RESOURCES TABLE
- EXPERIMENTAL MODEL AND STUDY PARTICIPANT DETAILS
  - Cell strains
  - E. *coli* cell culture
  - U2OS cell culture
- METHOD DETAILS
  - Protein purification from E. *coli* cells
  - UnaG labeling
  - Phase separation assays
  - Turbidity assay
  - FRAP assays
  - Cloning, knock-in editing, and knock-in validation in U2OS cells
  - Live cell imaging and FRAP assay
  - Electrophoretic mobility shift assays
- QUANTIFICATION AND STATISTICAL ANALYSIS
  - *In vitro* FRAP analysis
  - Live cell FRAP analysis
  - Electrophoretic mobility shift quantification

SUPPLEMENTAL INFORMATION

Supplemental information can be found online at https://doi.org/10.1016/j.crmeth.2025.101029.

Received: July 8, 2024
Revised: February 3, 2025
Accepted: March 27, 2025
Published: April 21, 2025

REFERENCES

1. Hancock, R., and Jeon, K.W. (2014). Preface. New models of the cell nucleus: crowding, entropic forces, phase separation, and fractals. Int. Rev. Cell Mol. Biol. *307*, xiii. https://doi.org/10.1016/B978-0-12-800046-5.10000-1.
2. Banani, S.F., Lee, H.O., Hyman, A.A., and Rosen, M.K. (2017). Biomolecular condensates: organizers of cellular biochemistry. Nat. Rev. Mol. Cell Biol. *18*, 285–298. https://doi.org/10.1038/nrm.2017.7.
3. Wang, B., Zhang, L., Dai, T., Qin, Z., Lu, H., Zhang, L., and Zhou, F. (2021). Liquid-liquid phase separation in human health and diseases. Signal Transduct. Targeted Ther. *6*, 290. https://doi.org/10.1038/s41392-021-00678-1.
4. Andre, A.A.M., and Spruijt, E. (2020). Liquid-Liquid Phase Separation in Crowded Environments. Int. J. Mol. Sci. *21*, 5908. https://doi.org/10.3390/ijms21165908.
5. Alberti, S., Gladfelter, A., and Mittag, T. (2019). Considerations and Challenges in Studying Liquid-Liquid Phase Separation and Biomolecular Condensates. Cellule *176*, 419–434. https://doi.org/10.1016/j.cell.2018.12.035.
6. Narlikar, G.J. (2020). Phase separation in chromatin organization. J. Bio. Sci. *45*, 5.
7. Kilic, S., Bachmann, A.L., Bryan, L.C., and Fierz, B. (2015). Multivalency governs HP1alpha association dynamics with the silent chromatin state. Nat. Commun. *6*, 7313. https://doi.org/10.1038/ncomms8313.
8. Larson, A.G., Elnatan, D., Keenen, M.M., Trnka, M.J., Johnston, J.B., Burlingame, A.L., Agard, D.A., Redding, S., and Narlikar, G.J. (2017). Liquid droplet formation by HP1alpha suggests a role for phase separation in heterochromatin. Nature *547*, 236–240. https://doi.org/10.1038/nature22822.
9. Canzio, D., Liao, M., Naber, N., Pate, E., Larson, A., Wu, S., Marina, D.B., Garcia, J.F., Madhani, H.D., Cooke, R., et al. (2013). A conformational switch in HP1 releases auto-inhibition to drive heterochromatin assembly. Nature *496*, 377–381. https://doi.org/10.1038/nature12032.
10. Wang, L., Gao, Y., Zheng, X., Liu, C., Dong, S., Li, R., Zhang, G., Wei, Y., Qu, H., Li, Y., et al. (2019). Histone Modifications Regulate Chromatin Compartmentalization by Contributing to a Phase Separation Mechanism. Mol. Cell *76*, 646–659.e6. https://doi.org/10.1016/j.molcel.2019.08.019.
11. Cheutin, T., McNairn, A.J., Jenuwein, T., Gilbert, D.M., Singh, P.B., and Misteli, T. (2003). Maintenance of stable heterochromatin domains by dynamic HP1 binding. Science *299*, 721–725. https://doi.org/10.1126/science.1078572.
12. Muller, K.P., Erdel, F., Caudron-Herger, M., Marth, C., Fodor, B.D., Richter, M., Scaranaro, M., Beaudouin, J., Wachsmuth, M., and Rippe, K. (2009). Multiscale analysis of dynamics and interactions of heterochromatin protein 1 by fluorescence fluctuation microscopy. Biophys. J. *97*, 2876–2885. https://doi.org/10.1016/j.bpj.2009.08.057.
13. Erdel, F., Rademacher, A., Vlijm, R., Tünnermann, J., Frank, L., Weinmann, R., Schweigert, E., Yserentant, K., Hummert, J., Bauer, C., et al. (2020). Mouse Heterochromatin Adopts Digital Compaction States without Showing Hallmarks of HP1-Driven Liquid-Liquid Phase Separation. Mol. Cell *78*, 236–249.e7. https://doi.org/10.1016/j.molcel.2020.02.005.
14. Strom, A.R., Biggs, R.J., Banigan, E.J., Wang, X., Chiu, K., Herman, C., Collado, J., Yue, F., Ritland Politz, J.C., Tait, L.J., et al. (2021). HP1alpha is a chromatin crosslinker that controls nuclear and mitotic chromosome mechanics. Elife *10*, e63972. https://doi.org/10.7554/eLife.63972.
15. Kumagai, A., Ando, R., Miyatake, H., Greimel, P., Kobayashi, T., Hirabayashi, Y., Shimogori, T., and Miyawaki, A. (2013). A bilirubin-inducible fluorescent protein from eel muscle. Cell *153*, 1602–1611. https://doi.org/10.1016/j.cell.2013.05.038.
16. Poudyal, M., Patel, K., Gadhe, L., Sawner, A.S., Kadu, P., Datta, D., Mukherjee, S., Ray, S., Navalkar, A., Maiti, S., et al. (2023). Intermolecular interactions underlie protein/peptide phase separation irrespective of

sequence and structure at crowded milieu. Nat. Commun. *14*, 6199. https://doi.org/10.1038/s41467-023-41864-9.

17. Li, C.H., Coffey, E.L., Dall'Agnese, A., Hannett, N.M., Tang, X., Henninger, J.E., Platt, J.M., Oksuz, O., Zamudio, A.V., Afeyan, L.K., et al. (2020). MeCP2 links heterochromatin condensates and neurodevelopmental disease. Nature *586*, 440–444. https://doi.org/10.1038/s41586-020-2574-4.
18. Andre, A.A.M., Yewdall, N.A., and Spruijt, E. (2023). Crowding-induced phase separation and gelling by co-condensation of PEG in NPM1-rRNA condensates. Biophys. J. *122*, 397–407. https://doi.org/10.1016/j.bpj.2022.12.001.
19. Keenen, M.M., Brown, D., Brennan, L.D., Renger, R., Khoo, H., Carlson, C.R., Huang, B., Grill, S.W., Narlikar, G.J., and Redding, S. (2021). HP1 proteins compact DNA into mechanically and positionally stable phase separated domains. Elife *10*, e64563. https://doi.org/10.7554/eLife.64563.
20. Phanindhar, K., and Mishra, R.K. (2023). Auxin-inducible degron system: an efficient protein degradation tool to study protein function. Biotechniques *74*, 186–198. https://doi.org/10.2144/btn-2022-0108.
21. Yeh, J.T.H., Nam, K., Yeh, J.T.H., and Perrimon, N. (2017). eUnaG: a new ligand-inducible fluorescent reporter to detect drug transporter activity in live cells. Sci. Rep. *7*, 41619. https://doi.org/10.1038/srep41619.
22. Schmiedeberg, L., Weisshart, K., Diekmann, S., Meyer Zu Hoerste, G., and Hemmerich, P. (2004). High- and low-mobility populations of HP1 in heterochromatin of mammalian cells. Mol. Biol. Cell *15*, 2819–2833. https://doi.org/10.1091/mbc.e03-11-0827.
23. Meshorer, E., Yellajoshula, D., George, E., Scambler, P.J., Brown, D.T., and Misteli, T. (2006). Hyperdynamic plasticity of chromatin proteins in pluripotent embryonic stem cells. Dev. Cell *10*, 105–116. https://doi.org/10.1016/j.devcel.2005.10.017.
24. Strom, A.R., Emelyanov, A.V., Mir, M., Fyodorov, D.V., Darzacq, X., and Karpen, G.H. (2017). Phase separation drives heterochromatin domain formation. Nature *547*, 241–245. https://doi.org/10.1038/nature22989.
25. Spegg, V., Panagopoulos, A., Stout, M., Krishnan, A., Reginato, G., Imhof, R., Roschitzki, B., Cejka, P., and Altmeyer, M. (2023). Phase separation properties of RPA combine high-affinity ssDNA binding with dynamic condensate functions at telomeres. Nat. Struct. Mol. Biol. *30*, 451–462. https://doi.org/10.1038/s41594-023-00932-w.
26. Wegmann, S., Eftekharzadeh, B., Tepper, K., Zoltowska, K.M., Bennett, R.E., Dujardin, S., Laskowski, P.R., MacKenzie, D., Kamath, T., Commins, C., et al. (2018). Tau protein liquid-liquid phase separation can initiate tau aggregation. EMBO. J. *37*, e98049. https://doi.org/10.15252/embj.201798049.
27. Soltys, K., and Ozyhar, A. (2023). Phase separation propensity of the intrinsically disordered AB region of human RXRbeta. Cell Commun. Signal. *21*, 92. https://doi.org/10.1186/s12964-023-01113-4.
28. Junjiao Yang, C.-I.C., Koach, J., Liu, H., Navalkar, A., Zhao, Q., Yang, X., He, L., Mittag, T., Yin, S., Weiss, W.A., and Shu, X. (2022). Phase separation of Myc differentially modulates the transcriptome. Preprint at bioRxiv. https://doi.org/10.1101/2022.06.28.498043.
29. Cieplak, A.S. (2023). In Protein Aggregation Methods and Protocols, J.M. Walker, ed. (Springer Protoco).

STAR★METHODS

KEY RESOURCES TABLE

REAGENT or RESOURCE	SOURCE	IDENTIFIER
Bacterial and virus strains		
BL21-Gold (DE3) competent cells	Agilent Technology	230132
Rosetta competent cells	Millipore Sigma	70954
Chemicals, peptides, and recombinant proteins		
Bilirubin	Sigma Aldrich	B4126-1G
PEG8000	RPI	P48080
PEG4000	Sigma	8.07490
Experimental models: Cell lines		
U2OS cells	ATCC	HTB-96
Oligonucleotides		
Forward primer hCBX5 F: CTCCTTTTAAGTCTCATATTCTTTCTCTCCAGG	IDT	Custom order
Reverse primer hCBX5 R: GAGGAGGCAGGGAGGTGAATGTATTATGTAC	IDT	Custom order
Recombinant DNA		
PBH4-6xHis-hHP1α	Larson et al.[8]	N/A

EXPERIMENTAL MODEL AND STUDY PARTICIPANT DETAILS

Cell strains

The experimental model is E. *coli* Rosetta for generating recombinant wild-type HP1α and HP1α-KCK. The experimental model is E. *coli* BL21-Gold (DE3) for generating all the tagged HP1α constructs. Proteins used in all the biochemical assays, including phasing, turbidity, FRAP, and electron mobility shift assays, were generated from one of the two E. *coli* strains described above. Wild type U2OS cells were used to generate endogenously tagged HP1α proteins, knock-in details under STAR Methods section ''Cell culture, cloning, knock-in editing, and knock-in validation''.

E. *coli* cell culture

All HP1α tagged constructs with a 6x-His tag on the N-terminus were ordered from Genscript cloned into a PBH4 parent vector derived from Larson et al.[8] Rosetta competent cells (Millipore Sigma 70954) were transformed with expression vectors for 6x-HIS HP1α, and BL21-Gold (DE3) competent cells (Agilent Technology 230132) were transformed with expression vectors for all other 6x-HIS HP1α tagged constructs (mEGFP, UnaG, AID-sfGFP, AID). Both cells were grown in 2xLB supplemented with 25 μg/mL carbenicillin at 37 C to an OD600 of 0.3–0.4 then moved to 18 C and then allowed to grow till the OD600 reached 0.6–0.8, before inducing with 0.8 mM isopropy-β D-thiogalactopyranoside (IPTG). Cells were then grown overnight for 16–20 h at 18 C, before pelleting at 4000xg for 30 min. Cell pellets were collected using a spatula and flash frozen in liquid nitrogen and stored at 80 C until the day of purification.

U2OS cell culture

U2OS cells (ATCC HTB-96) were cultured in a CELLSTAR T-25 flask (Greiner Bio One 690175) with McCoy's 5A modified medium (Gibco 16600082) supplemented with 10% FBS (UCSF Cell Culture Facility), 1x GlutaMax (Gibco 35050061), 1 mM Sodium Pyruvate (HyClone SH30239), and Streptomycin/Penicillin (UCSF Cell Culture Facility) for every 48–72 h in a 37 C and 5% CO_2 incubator.

METHOD DETAILS

Protein purification from E. *coli* cells

Each pellet was resuspended and thawed in lysis/wash buffer (1x PBS, 300 mM KCl,10% Glycerol, 7.5 mM Imidazole), supplemented with protease inhibitors (1 μg/mL pepstatin A (Gold Biotechnology P-020-100), 1 mM phenylmethanesulfonyl fluoride (Sigma-Aldrich 78830), and 3 μg/mL leupeptin (Sigma-Aldrich L2884)). Cells were lysed using a C3 Emulsiflex (ATA Scientific). Lysate was clarified by centrifugation at 30,000xg for 40 min in Oakridge tubes. The supernatant was bound to of Talon cobalt resin (Takara 635636) on rotation for 1–1.5 h. The bound resin was batch-washed with the lysis/wash buffer for 60x the resin volume. Protein was eluted in of

elution buffer (20 mM HEPES pH 7.5, 100 mM KCl, 400 mM Imidazole). TEV protease was added to the eluted protein and allowed to dialyze overnight in dialysis buffer (20 mM HEPES pH 7.5, 150 mM KCl, 3 mM DTT). The cleaved protein was filtered through a 0.22 μm filter and then further purified through anion exchange, using a Mono Q 10/100 GL column (GE Healthcare). The protein was eluted using a salt gradient, from 80 mM to 1 M KCl over 20 column volumes in buffer containing 20 mM HEPES pH 7.5 and 3 mM DTT. The fractions containing protein were pooled and concentrated in a 10K Amicon Ultra-4 spin concentrator (Millipore 234753) down to 500 μL. The protein was injected onto a Superdex-75 Increase 10/300 GL column (GE Healthcare 29148721) for size exclusion chromatography in SEC buffer (20 mM HEPES pH 7.5, 10% Glycerol, 300 mM KCl, 3 mM DTT). Fractions containing protein were pooled and concentrated again, aliquots were then flash-frozen and stored at 80 C.

All HP1α constructs were purified as described above. Minor changes were made for the tagged constructs that are larger than 50 kDa. During concentration, a 30K Amicon Ultra-4 spin concentrator (Millipore 216718) was used instead of a 10K concentrator. For size exclusion chromatography, a Superdex-200 Increase 10/300 GL column (Cytiva 28-9909-44) was used instead of a Superdex-75 increase column.

UnaG labeling

A stoichiometry of 2:1 Bilirubin (Sigma Aldrich B4126-1G) to protein was added to purified HP1α-8aa-UnaG and HP1α-16aa-UnaG. The protein-dye mixture was incubated for 15 min on ice before separating the unbound Bilirubin on a PD10 desalting column.

Phase separation assays

Greiner Sensoplate glass bottom 384-well plates (Sigma-Aldrich M4187) were used for the visualization of phase-separated droplets in this study. The wells in the plates were first washed 2 times with 100 μL of water, then with 100 μL of 2% Hellmanex (Sigma-Aldrich Z805939) for 30 min, followed by three water rinses. Next, 100 μL of 0.5M NaOH was added to each well for 30 min, followed by another water rinse. Afterward, 70 μL of 20 mg/mL PEG-silane MW-5000 (Laysan Bio MPEG-SIL-5000) dissolved in 95% EtOH was added to each well and allowed to sit overnight at 4 *C*, away from light. The next day, 30 μL of 95% EtOH was added to each well and the wells were washed 2 times with 95% EtOH, but not left dry for more than 5 s. After the EtOH wash step, the wells were washed 3-times with water. Next, 100 μL of 100 mg/mL of BSA (Sigma A4503-50G) was added to each well and allowed for a 30-min incubation. The wells were washed extensively (5 times) with water and 2 times with assay buffer (20 mM HEPES pH 7.5, 70 mM KCl, 1 mM DTT).

Both HP1α constructs and DNA were dialyzed into phasing buffer (20 mM HEPES pH 7.5, 70 mM KCl, 1 mM DTT) overnight prior to the experiment. Samples were calculated to be 2x each and added to PCR tubes on ice for 20 min for a final concentration of 1x and a total volume of 15–30 μL. For all condensates induced by PEG8000 (RPI P48080) or PEG4000 (Sigma 8.07490), 100 mg/mL was used as 10% PEG. The assay buffer remaining in the wells was rapidly removed, and samples were immediately added into the wells, one condition at a time. The droplets were allowed to settle at room temperature for 1 h before imaging. All experiments were performed in triplicate. The settled non-fluorescent condensates were visualized by bright field microscopy at 20x magnification using the 6D/High throughput microscope at the Nikon imaging center at UCSF (except for MBP which was imaged at 40x magnification). Fluorescently tagged HP1α constructs were visualized using the same microscope but using the FITC channel instead of brightfield.

Turbidity assay

Greiner Sensoplate glass bottom 384-well plates (Sigma-Aldrich M4187) were used for the A340 reading in this study. Each concentration dependence was carried out in triplicate using the same reaction preparation methods described in the previous section except that the plates were not pre-coated with PEG-silane. The plate was incubated at room temperature for 10 min after sample addition, and absorbance was measured at 340 nm using a Spectramax M5 plate reader. Saturation concentrations were not derived for constructs that did not phase separate (as validated through light microscopy). The saturation concentrations for constructs that underwent phase separation were determined as follows. One line was fit to the shallow region of the data while another line was fit to the steep region of the data. The saturation concentration was determined from the intersection of the two lines. The data are thus used to find the inflection point where the A340 absorbance starts rising steeply. An example of how the data was fitted is shown in Figure S4G (Figure S4G). Three independent datasets were used to derive the saturation concentrations for each condition. These saturation concentrations are reported in Tables S3 and S4 along with the associated standard deviation for each set of the three conditions.[29]

FRAP assays

Droplets used for FRAP were prepared using the methods above, however, imaging was done using the Crest LFOV Spinning Disk/C2 Confocal microscope at 100x magnification at room temperature. For non-PEG condensates, a final concentration of 10 μM of HP1α and HP1α-16aa-UnaG were mixed with 30 nM of 2.7 kbp DNA. For all PEG-induced condensates, the same final concentration of HP1α, HP1α tag constructs, and DNA were used, with 10% PEG. All condensates were photobleached in the GFP-FRAP channel, using 10% 405 nm laser power. A round region of interest (ROI) was drawn on the area of interest for bleaching and assigned to the setting as described below. For all droplets, dwell time was set to 200 μs. Three images were captured before photobleaching, for an interval of 300 msec, followed by 200 msec stimulation of bleaching. Without delay, 15 s of images were taken with 50 loops, and then 1 s intervals for more images for another 30 s. After stimulation, the same ROI was replicated two times, where one was placed in a

background area, and the other one placed on a droplet that had not been bleached. All intensity values were measured using the Element software and exported to Excel. To normalize intensity, an equation was used (Bleached ROI intensity – Background ROI intensity)/(non-bleached droplet ROI intensity - Background ROI intensity).

Whole droplet FRAP samples were prepared, imaged, and calculated using the methods above and the equation below. A larger round region of interest (ROI) was drawn and duplicated to cover all areas of bleached droplets. Four images were captured before photobleaching, for an interval of 600 msec, followed by 8000 msec stimulation of bleaching. Without delay, 30 s of images were taken with 150 loops, and then 1 s intervals for more images for another 130 s.

Cloning, knock-in editing, and knock-in validation in U2OS cells

Plasmids containing homology arm sequences for HP1α 3′ end and donor sequences of UnaG or eUnaG were cloned with fluorescent protein cDNAs (IDT) and human 3′ HP1α-AID-sfGFP 2A PuroR (Addgene 127906). U2OS cells with 50% confluency in a T-25 flask were co-transfected with pX330 human 3′ HP1α-gRNA/Cas9 (Addgene 127907) and pX330 human 3′ HP1α-16aa-UnaG or eUnaG plasmids with JetOptimus (PolyPlus 10100025) according to manufacturer's instructions. After 24 h of transfection, edited cells were sorted by FACS (BD FACS Aria Fusion 1, Gladstone Institute) and collected in collection buffer (10% FBS, 1x Streptomycin/Penicillin in PBS), then cultured for further experiments. To obtain most homozygous knock-in cell populations, <10% of edited cells with the highest green fluorescence intensity upon 488 nm excitation wavelength (with 530/30 bandpass filter) were sorted twice or more. Knock-in was validated by genomic DNA PCR/sequencing and fluorescent microscopy.

Primer sequences flanking to human HP1α (CBX5) exon 5 and stop codon used for genomic DNA PCR validation are as follows:

Forward primer hCBX5 F: CTCCTTTTAAGTCTCATATTCTTTCTCTCCAGG.

Reverse primer hCBX5 R: GAGGAGGCAGGGAGGTGAATGTATTATGTAC.

Live cell imaging and FRAP assay

Cultured cells were trypsinized and resuspended in McCoy's 5A modified medium, then 50,000 of cells were seeded in an 8-well chambered cover glass (CellVis C8-1.5P) the day before imaging. Prepared cell samples were incubated in a 37 C, 5% CO_2 incubator overnight. Chambered slide glasses were passivated with poly-L-lysine (Sigma-Aldrich P4707) before cell seeding. Before imaging, the media was discarded, and cells were washed twice with PBS (UCSF Cell Culture Facility). For DNA staining, cells were incubated with 1:2000 diluted Hoechst 33342 (Invitrogen H3570) in PBS solution for 10 min, then the media was further changed to 75 mM HEPES (Corning 25060CI) in FluoroBrite DMEM (Gibco A1896701) supplemented with 1x GlutaMax for imaging. The live cell-containing chambered cover glass was mounted in a 37 C, 5% CO_2 incubation chamber (Okolab). All live cell images were acquired using a CSU-W1 spinning disk LFOV (Large Field of View) high-speed confocal microscope at the Nikon Imaging Center at UCSF, with a Plan Apo λ 60x/NA 1.4 oil immersion objective lens and Zyla 4.2 sCMOS (Andor) for 2-channel imaging or iXon Ultra DU-888 EMCCD (Andor) for FRAP experiments on an inverted Eclipse Ti (Nikon) microscope body.

For 2-channel (Hoechst for DNA and HP1α-16aa-FP) imaging, 405 nm and 488 nm laser (Voltran) were used to excite Hoechst and HP1α-16aa-UnaG or HP1α-16aa-eUnaG puncta in cells. 41 z-slices of both Hoechst and FP channel images were imaged with 0.26 μm steps, ranging 10.40 μm, and representative images were processed with maximum intensity projection.

For FRAP experiments, a target puncta-including region of interest (ROI) in the selected U2OS HP1α-16aa-UnaG and HP1α-16aa-eUnaG Knock-in cells was stimulated with 405 nm laser (Voltran) for 200 msec bleaching time with 30 mW laser power. Every time-lapsed image was captured with a 500 msec interval, and 100 consecutive images were acquired with a 300 msec of exposure time at 6% 488 nm laser power for a total of 50 s. The first three images were captured before photobleaching without any delays.

Electrophoretic mobility shift assays

Reactions contained HP1α or tagged HP1α at various concentrations (stated in the figure legend), with 20 nM of Cy5 labeled 187 bp DNA in phasing buffer (20 mM HEPES pH 7.5, 70 mM KCl, 1 mM DTT). Reactions were carried out on ice but allowed to incubate at room temperature for 15 min before loading. A final concentration of 10% glycerol was added to reactions after incubation and bound and unbound DNA was separated by electrophoresis on a 6% acrylamide, 0.5X TBE native gel for 3 h. The gel was imaged on an Amersham Typhoon laser-scanner platform (29187191) in the Cy5 channel.

QUANTIFICATION AND STATISTICAL ANALYSIS

In vitro FRAP analysis

The *in vitro* FRAP data was averaged and fitted to the following equation:

$$Y = Y_0 + \text{SpanFast}\left(1 \quad e^{(-\text{KFast } X)}\right) + \text{SpanSlow}\left(1 \quad e^{(-\text{KSlow } X)}\right)$$

$$\text{SpanFast} = (\text{Plateau} \quad \text{Y0})\ \text{PercentFast}\ .01$$

$$\text{SpanSlow} = (\text{Plateau} \quad \text{Y0})\ (100 \quad \text{PercentFast})\ .01$$

Constraint: Plateau was set to 1.

To collect Fraction long-term recovery data, the constraint was deleted and the same equations above were used.

Live cell FRAP analysis

All intensity values in the time-lapse images were analyzed with ImageJ software. The bleached ROI was masked, and the region of bleached puncta within the bleached ROI was captured by Gaussian blurring (1 sigma) and thresholding with the Otsu thresholding algorithm embedded in ImageJ. Fluorescence intensities of pixels in the region of bleached puncta were averaged and determined as I_{puncta}. All HP1α-16aa-UnaG or HP1α-16aa-eUnaG puncta within the bleached cell were detected with the same thresholding algorithm. All detected puncta were enlarged by 1 pixel to include puncta-nucleoplasm interface pixels. All detected puncta were merged for masking total puncta to determine average nucleoplasm intensity (the bleached cell – total puncta in the bleached cell) I_{nuc}. Background offset I_{bg} was determined by measuring and averaging intensities of the regions excluding cells in the image of analysis.

For the correction of time-resolved global photobleaching during imaging, we measured and averaged the fluorescence intensities of pixels in all cells excluding the bleached cell in the image, to set I_{ref} as a correction factor for photobleaching.

The corrected intensity ratio is

$$I_{corr(t)} = I_{puncta}(t) - I_{nuc}(t) / I_{ref}(t) - I_{bg}(t)$$

For the normalization for FRAP curve fitting, the average I_{corr} of the first three pre-bleached images was set to 1, and $I_{corr}(t = 0)$ of the first image after photobleaching was set to 0 for the normalization.

The data was averaged and fitted to the same equation as *in vitro* FRAP analysis.

Electrophoretic mobility shift quantification

Fraction unbound was quantified in Fiji as a function of increasing concentration of protein and the following equation was fit to the data:

$$\text{Fraction unbound} = [HP1^{n} / [HP1^{n} + [K_{1/2}]^{n}$$